Journal of
Mechanics of
Materials and Structures

A GENERALIZED PLANE STRAIN MESHLESS LOCAL PETROV–GALERKIN METHOD FOR THE MICROMECHANICS OF THERMOMECHANICAL LOADING OF COMPOSITES

Isa Ahmadi and Mohamad Aghdam

Volume 5, No. 4 April 2010

mathematical sciences publishers

JOURNAL OF MECHANICS OF MATERIALS AND STRUCTURES
Vol. 5, No. 4, 2010

A GENERALIZED PLANE STRAIN MESHLESS LOCAL PETROV–GALERKIN METHOD FOR THE MICROMECHANICS OF THERMOMECHANICAL LOADING OF COMPOSITES

ISA AHMADI AND MOHAMAD AGHDAM

A generalized plane strain micromechanical model is developed to predict the behavior of a unidirectional fiber-reinforced composite subjected to combined thermal and mechanical loads. An appropriate meshless local Petrov–Galerkin formulation is presented for the solution of the governing partial differential equations of the problem. To reduce computation time, a unit step function is employed as test function. A direct method is presented for enforcement of the continuity of displacement and traction at the fiber-matrix interface to model the fully bonded interface. Results of this study revealed that the model provides highly accurate predictions with relatively small number of nodes. Numerical results for glass/epoxy and SiC/Ti composites subjected to thermomechanical loading show that predictions for both local and global responses of the composites are in good agreement with results of theoretical, experimental and finite element methods.

1. Introduction

During the past decade, the idea of using meshless methods for the solution of boundary value problems has received much attention and undergone significant progress. In meshless methods, no predefined mesh of elements is needed between the nodes for the construction of a trial or test function. One of the main objectives of such methods is to eliminate or alleviate difficulties inherent to meshing and remeshing of the domain, or the locking and distortion of elements.

Various meshless methods such as the diffuse element method [Nayroles et al. 1992], the element-free Galerkin (EFG) method [Belytschko et al. 1994], the reproducing kernel particle method [Liu et al. 1996], the meshless local boundary integral equation (LBIE) method [Zhu et al. 1998], and the meshless local Petrov–Galerkin (MLPG) method [Atluri and Zhu 1998] have been developed in the last two decades. In some of them, such as EFG, a background mesh is required for integration of the weak form of equations. By contrast, MLPG requires no mesh either for the interpolation of the solution variable or for the integration of the weak form of equations. Some applications of this promising, efficient and flexible method include solving Poisson's equation [Atluri and Zhu 1998], elastostatic and elastodynamic problems [Atluri and Zhu 2000; Long et al. 2006], plate bending [Gu and Liu 2001], fracture mechanics [Ching and Batra 2001], and Navier–Stokes flow [Lin and Atluri 2001; Atluri and Shen 2002].

On the other hand, various techniques both analytical [Gramoll et al. 1991; Arsenault and Taya 1987; Yeh and Krempl 1993; Uemura et al. 1979; Brayshaw and Pindera 1994; Tsai and Chi 2008]

Keywords: meshless local Petrov–Galerkin method, MLPG, generalized plane strain, micromechanics, metal-matrix composite, thermal residual stress.

and numerical have been used in the micromechanical analysis of heterogeneous materials. Though approaches based on the finite difference and boundary element methods can be found in the literature (see [Adams and Doner 1967] and [Eischen and Torquato 1993], respectively), most numerical approaches rely on the finite element method [Nimmer 1990; Nimmer et al. 1991; Wisnom 1990; Durodola and Derby 1994; Shaw and Miracle 1996; Zhang et al. 2004; Dvorak et al. 1973; Zahl and McMeeking 1991; Aghdam et al. 2000; Aghdam and Khojeh 2003; Gentz et al. 2004; Zhao et al. 2007; Shen 1998; Haktan Karadeniz and Kumlutas 2007], and have been used for predicting various elastic, elastoplastic and thermoelastic characteristics of composites.

Some of these models include the effect of thermal stress on the mechanical behavior of composite materials. In addition to [Durodola and Derby 1994; Shaw and Miracle 1996], we mention [Nimmer 1990; Nimmer et al. 1991; Wisnom 1990], where it was found that residual stresses at the interface of the fiber and matrix are compressive and therefore they are beneficial for the transverse behavior of the MMCs with weak interface. Shaw and Miracle [1996] used the finite element method to study the effects of interfacial region on the thermal residual stress and transverse behavior of a SiC/Ti metal-matrix composite. The influence of residual stresses on the yielding behavior of composite materials was studied in [Dvorak et al. 1973; Zahl and McMeeking 1991; Aghdam et al. 2000; Aghdam and Khojeh 2003], while [Gentz et al. 2004] and [Zhao et al. 2007] studied the effects of the residual stresses on the behavior of polymer-matrix composite. In addition, the overall coefficient of thermal expansion of composite materials was studied using micromechanical finite element [Shen 1998; Haktan Karadeniz and Kumlutas 2007], approximate closed-form models [Van Fo Fy 1965; Rogers et al. 1977; Chamis 1984], and experimental methods [Sideridis 1994].

More recently, Dang and Sankar [2007] employed the conventional MLPG method for the micromechanical analysis of unidirectional composites. They used the penalty parameter method to enforce the essential boundary conditions on the RVE. Their predictions show reasonably good agreement with finite element results. However, the conventional MLPG formulation with Gaussian weight functions and transformation technique in their paper seems to be time-consuming and computationally expensive due to a domain integration in the weak formulation.

In this study, a micromechanical model based on the generalized plane strain assumption is developed to study the behavior of unidirectional composites subjected to thermomechanical loading. An appropriate meshless local Petrov–Galerkin (MLPG) formulation is presented for the generalized plane strain case in the presence of thermal loading. This formulation is used to solve the governing equations of the system. A unit step function is considered as the test function, which leads to the elimination of domain integration in the absence of body forces and therefore, to the reduction in the computational cost. A direct interpolation method is introduced for the enforcement of the displacement continuity and traction reciprocity conditions at the fiber-matrix interface based on the fully bonded interface assumption. These continuity conditions are imposed directly on the discretized equation.

The method presented is used to predict the thermal residual stress in SiC/Ti metal-matrix composites resulting from the manufacturing process, and the effects of these stresses on the total stress distribution due to the mechanical loading of the SiC/Ti composite. Comparison of the predictions for the overall coefficient of thermal expansion and the displacement and stress components show excellent agreement with other experimental, finite element and approximate closed-form analyses. Numerical analysis suggests that the model can provide highly accurate results with a relatively small number of nodes.

2. Analysis

2.1. ***Micromechanical model.*** The micromechanical analysis of a unidirectional fiber-reinforced composite subjected to a combined normal and thermal loading can be modeled using a generalized plane strain assumption [Wisnom 1990] instead of a 3D elasticity model. In the generalized plane strain condition displacement occurs in all three directions, except that strain components are not functions of the x_3 coordinate (fiber direction) and the normal strain in the x_3-direction is constant (Figure 1). Therefore, the displacement fields within the domain based on the generalized plane strain assumption should be considered as

$$u_1 = u_1(x_1, x_2), \quad u_2 = u_2(x_1, x_2), \quad u_3 = \varepsilon_0 x_3, \tag{1}$$

where u_1, u_2 and u_3 are the displacements in x_1, x_2 and x_3 directions, respectively, and ε_0 is an unknown normal constant strain in x_3-direction to be determined. Using the displacement field (1), the strain-displacement relations based on the linear theory of elasticity can be obtained as

$$\varepsilon_{11} = \frac{\partial u_1}{\partial x_1}, \quad \varepsilon_{22} = \frac{\partial u_2}{\partial x_2}, \quad \varepsilon_{33} = \frac{\partial u_3}{\partial x_3} = \varepsilon_0, \quad \varepsilon_{12} = \frac{1}{2}\left(\frac{\partial u_1}{\partial x_2} + \frac{\partial u_2}{\partial x_1}\right), \quad \varepsilon_{13} = 0, \quad \varepsilon_{23} = 0. \tag{2}$$

Using (2), one can conclude that the out-of-plane shear stresses vanish: $\sigma_{13} = \sigma_{23} = 0$. The governing equilibrium equations of the problem in the x_1- and x_2-directions in the absence of shear stresses σ_{13} and σ_{23} can be considered as

$$\sigma_{ij,j} + b_i = 0 \quad \text{on } \Omega, \quad i, j = 1, 2, \tag{3}$$

in which $\sigma_{ij,j}$ is the partial derivative of the stress component σ_{ij} with respect to x_j, b_i is the body force in x_i-direction and Ω is the solution domain. Note that the equilibrium equation in the x_3 (fiber) direction in the absence of body force b_3 is automatically satisfied as $\sigma_{13} = \sigma_{23} = 0$ and the σ_3 stress are independent of the x_3 coordinate.

2.2. ***Solution domain.*** In most micromechanical models, a periodic arrangement of fibers is assumed in the composite and therefore, the smallest repeating area of the cross section of the composite known as the representative volume element (RVE) is considered as the solution domain. It is assumed further that the global behavior of the composite is the same as that of the RVE. Here a quarter of the fibers and corresponding matrix in a square array of fiber arrangement is selected as the RVE, as shown on the right in Figure 1.

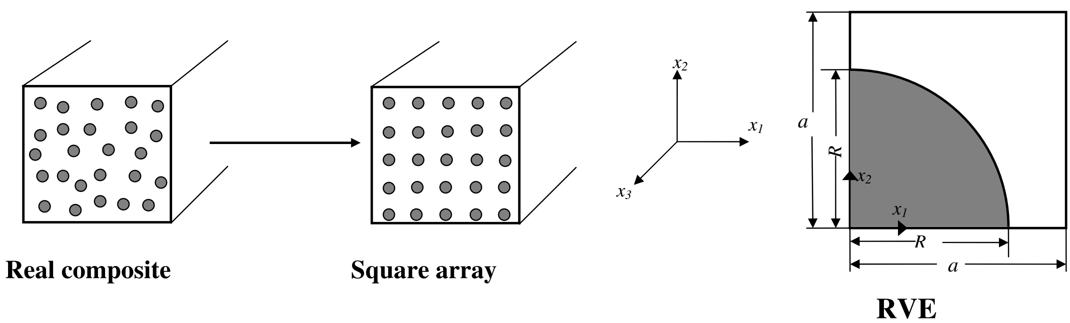

Figure 1. Left: real and idealized composite cross section (square array distribution). Right: the corresponding RVE.

2.3. ***Boundary and interface conditions.*** The boundary conditions must be set in such a way that the compatibility of the unit cell with neighboring cells in the infinite composite could be satisfied. For the thermomechanical loading of the composite in the absence of shear loading, the bottom edge of the RVE (x_1-axis) were not allowed to move in the x_2-direction and the left edge (x_2-axis) not allowed to move in the x_1-direction (Figure 1). The right edge can have an equal amount of the displacement in x_1-direction and the top edge can have an equal displacement in x_2-direction, so the nodes on right edge must be coupled in the x_2-direction. Similarly, the nodes on the top edge must be coupled in the x_1-direction. Therefore, appropriate boundary conditions on the various edges of the RVE can be considered as

$$\begin{aligned}
&\text{at } x_1 = 0: \quad u_1(0, x_2) = 0, \quad \sigma_{12} = 0, \\
&\text{at } x_1 = a: \quad u_1(a, x_2) = \bar{u}_1, \quad \sigma_{12} = 0, \quad \frac{1}{b}\int_{x_2=0}^{x_2=b} \sigma_1 dx_2 = \bar{\sigma}_1, \\
&\text{at } x_2 = 0: \quad u_2(x_1, 0) = 0, \quad \sigma_{12} = 0, \\
&\text{at } x_2 = b: \quad u_2(x_1, b) = \bar{u}_2, \quad \sigma_{12} = 0, \quad \frac{1}{a}\int_{x_1=0}^{x_1=a} \sigma_2 dx_1 = \bar{\sigma}_2, \quad \frac{1}{ab}\iint_{\Omega} \sigma_3 dx_1 dx_2 = \bar{\sigma}_3,
\end{aligned} \tag{4}$$

in which a is the length and b is the width of the RVE, $\bar{u}_i$ is the unknown constant displacement in the x_i-direction and $\bar{\sigma}_i$ is the applied transverse stress in the x_i-direction. The matrix is assumed to be perfectly bonded to the fibers throughout the analysis. This requires satisfaction of the continuity of displacements and reciprocity of traction at the fiber-matrix interface:

$$\boldsymbol{u}^f = \boldsymbol{u}^m, \quad \boldsymbol{t}^f + \boldsymbol{t}^m = 0, \tag{5}$$

where superscript f and m denote fiber and matrix, respectively, and $\boldsymbol{u}$ and $\boldsymbol{t}$ are the displacement and traction vectors on the interface. Solution of the governing equilibrium equation (3) together with the boundary conditions (4) in conjunction with the continuity of displacements and tractions at the interface (5) provides details of the distribution of various stress and strain components within the RVE.

3. Solution procedure

In this study, an appropriate Meshless Local Petrov–Galerkin (MLPG) formulation is presented for the generalized plane strain analysis of unidirectional composites subjected to thermomechanical loading. The MLPG solution procedure mainly includes three steps. 1- Approximation of the field variable $u(\boldsymbol{x})$ over randomly located nodes in the domain. 2- Converting the strong form of governing equations to the local symmetric weak form. 3- Numerical discretization of the weak form of the equations. In the first step the field variable must be approximated over the randomly distributed nodes and the trial functions must be constructed. One of the well-known methods for this purpose is the moving least squares (MLS) approximation technique [Atluri and Shen 2002] which is briefly described in the following section.

3.1. ***Moving least square (MLS) approximation.*** To approximate the distribution of the function $u(\boldsymbol{x})$ over a number of randomly located nodes within the domain by the MLS method, the unknown trial approximant $u^h(\boldsymbol{x})$ of the function $u(\boldsymbol{x})$ is defined as

$$u^h(\boldsymbol{x}) = \boldsymbol{p}^T(\boldsymbol{x})\boldsymbol{a}(\boldsymbol{x}), \quad \boldsymbol{x} \in \boldsymbol{\Omega}_{\boldsymbol{x}}, \tag{6}$$

where $\boldsymbol{p}^T(\boldsymbol{x}) = [p_1(\boldsymbol{x}), p_2(\boldsymbol{x}), \ldots, p_m(\boldsymbol{x})]$ is a complete monomial basis of order m and $\boldsymbol{a}(\boldsymbol{x})$ is a vector of unknown coefficients. For example, in a two-dimensional domain the complete monomial linear basis is $\boldsymbol{p}^T(\boldsymbol{x}) = [1, x_1, x_2]$, and the quadratic basis is $\boldsymbol{p}^T(\boldsymbol{x}) = [1, x_1, x_2, x_1^2, x_1x_2, x_2^2]$. In order to obtain the coefficients vector $\boldsymbol{a}(\boldsymbol{x})$, the weighted discrete norm

$$J(\boldsymbol{a}(\boldsymbol{x})) = \sum_{I=1}^{N} w_I(\boldsymbol{x})\big(\boldsymbol{p}^T(\boldsymbol{x}_I)\boldsymbol{a}(\boldsymbol{x}) - \hat{u}^I\big)^2 \tag{7}$$

should be minimized with respect to $\boldsymbol{a}(\boldsymbol{x})$. In (7) the $\hat{u}^I$ are fictitious nodal values of the field variable to be determined, w_I is a weigh function and N is the number of nodes in the neighborhood of $\boldsymbol{x}$ where the weight function vanishes: $w_I(\boldsymbol{x}) \neq 0$. In this study, quadratic spline functions are used:

$$w_I(\boldsymbol{x}) = \begin{cases} 1 - 6(d_I/r_I)^2 + 8(d_I/r_I)^3 - 3(d_I/r_I)^4 & \text{for } 0 \le d_I \le r_I, \\ 0 & \text{for } d_I \ge r_I, \end{cases} \tag{8}$$

where $d_I = |\boldsymbol{x} - \boldsymbol{x}_I|$ is the distance from the sampling point $\boldsymbol{x}$ to the node $\boldsymbol{x}_I$ and r_I is known as the radius of the domain of influence for the weight function $w_I(\boldsymbol{x})$ [Atluri and Shen 2002]. After obtaining $\boldsymbol{a}(\boldsymbol{x})$, one can determine from (6) the nodal interpolation form of $u^h(\boldsymbol{x})$:

$$u^h(\boldsymbol{x}) = \sum_{I=1}^{N} \phi^I(\boldsymbol{x})\hat{u}^I \quad \boldsymbol{x} \in \Omega_{\boldsymbol{x}}, \tag{9}$$

where $\phi^I(\boldsymbol{x})$ is the so-called shape function of the MLS approximation corresponding to node I and is defined as

$$\phi^I(\boldsymbol{x}) = \sum_{j=1}^{m} p_j(\boldsymbol{x})[\boldsymbol{A}^{-1}(\boldsymbol{x})\boldsymbol{B}(\boldsymbol{x})]_{jI}, \tag{10}$$

the matrices $\boldsymbol{A}(\boldsymbol{x})$ and $\boldsymbol{B}(\boldsymbol{x})$ being defined by

$$\boldsymbol{A}(\boldsymbol{x}) = \sum_{I=1}^{N} w_I(\boldsymbol{x})\boldsymbol{p}(\boldsymbol{x}_I)\boldsymbol{p}^T(\boldsymbol{x}_I), \tag{11}$$

$$\boldsymbol{B}(\boldsymbol{x}) = [w_1(\boldsymbol{x})\boldsymbol{p}(\boldsymbol{x}_1), w_2(\boldsymbol{x})\boldsymbol{p}(\boldsymbol{x}_2), \ldots, w_N(\boldsymbol{x})\boldsymbol{p}(\boldsymbol{x}_N)]. \tag{12}$$

Note that the shape functions derived from the MLS approximation are not orthonormal (that is, it need not be the case that $\phi^I(\boldsymbol{x}_J) = \delta_{IJ}$ and $u^h(\boldsymbol{x}_I) = \hat{u}^I$). Therefore, the enforcement of essential boundary conditions in the MLPG method has some difficulties and in the MLPG method, usually a penalty parameter or the Lagrange method is used for enforcement of the essential boundary conditions.

3.2. ***MLPG formulation.*** The MLPG method is based on the local weak form of the equations over the local subdomain Ω_s that is located inside the global domain Ω. The generalized local weak form (3) over the local subdomain of node I, Ω_s^I, can be written as

$$\int_{\Omega_s^I} (\sigma_{ij,j} + b_i)v_i \, d\Omega_s - \beta \int_{\Gamma_{su}^I} (u_i - \bar{u}_i)\, d\Gamma = 0, \tag{13}$$

where u_i and v_i are the trial and test (weight) functions, respectively, Γ_{su}^I is the part of the boundary of subdomain of node I i.e., $\partial\Omega_s^I$, over which the essential boundary conditions are specified and β is a large number which is known as penalty parameter and is employed in order to impose essential boundary conditions. Using the identity $\sigma_{ij,j}v_j = (\sigma_{ij}v_j)_{,j} - \sigma_{ij}v_{i,j}$ and applying the divergence theorem, the local symmetric weak form of (13) can be written as

$$\int_{\partial\Omega_s^I} \sigma_{ij}n_j v_i \, d\Gamma - \int_{\Omega_s^I} (\sigma_{ij}v_{i,j} - b_i v_i)\, d\Omega - \beta \int_{\Gamma_{su}^I} (u_i - \bar{u}_i) v_i \, d\Gamma = 0, \tag{14}$$

where n_j is the unit outward normal of the $\partial\Omega_s^I$. In general Ω_s^I could have arbitrary shape and $\partial\Omega_s^I$ consists of three parts: $\partial\Omega_s^I = L_s^I \cup \Gamma_{st}^I \cup \Gamma_{su}^I$, in which L_s^I, Γ_{st}^I and Γ_{su}^I are parts of the local boundary that are located totally inside the global domain, coincides with the global traction boundary and coincides with the global essential boundary, respectively. We can rewrite (14) in terms of L_s^I, Γ_{st}^I, and Γ_{su}^I as

$$\begin{aligned}\int_{\Omega_s^I} (\sigma_{ij}v_{i,j})\, d\Omega - \int_{L_s^I} t_i v_i \, d\Gamma - \int_{\Gamma_{su}^I} t_i v_i \, d\Gamma + \beta \int_{\Gamma_{su}^I} u_i v_i \, d\Gamma \\ = \int_{\Gamma_{st}^I} \bar{t}_i v_i \, d\Gamma + \beta \int_{\Gamma_{su}^I} \bar{u}_i v_i \, d\Gamma + \int_{\Omega_s^I} b_i v_i \, d\Omega,\end{aligned} \tag{15}$$

where $t_i = \sigma_{ij}n_j$ is the reaction vector on the boundary of the subdomain and $\bar{t}_i$ is the natural boundary condition on Γ_{st}^I. Unlike the conventional Galerkin method in which the trial and test functions are chosen from the same space, the Petrov–Galerkin method uses the trial and test functions from different spaces. In this study, in order to reduce the computational

time, the test functions v_i are chosen such that the domain integral on Ω_s^I is eliminated. This can be accomplished by using the unit step function as the test function in each subdomain as

$$v_i(\boldsymbol{x}) = \begin{cases} 1 & \text{for } \boldsymbol{x} \in \Omega_s^I, \\ 0 & \text{for } \boldsymbol{x} \notin \Omega_s^I. \end{cases} \tag{16}$$

It is clear that the partial derivatives of the unit step function are identically zero, and therefore, the corresponding domain integral in (15) is eliminated. The final form of the local symmetric weak form can be written as

$$-\int_{L_s^I} t_i \, d\Gamma - \int_{\Gamma_{su}^I} t_i \, d\Gamma + \beta \int_{\Gamma_{su}^I} u_i \, d\Gamma = \int_{\Gamma_{st}^I} \bar{t}_i \, d\Gamma + \beta \int_{\Gamma_{su}^I} \bar{u}_i \, d\Gamma + \int_{\Omega_s^I} b_i \, d\Omega. \tag{17}$$

Note that by ignoring the body forces, any domain integration is eliminated from (17).

3.3. ***Numerical discretization.*** Assuming a linear isotropic elastic behavior for both the fiber and matrix and the generalized plane strain condition, the compact form of the stress-strain relations in the presence of temperature change ΔT for each phase in the RVE can be written as

$$\left.\begin{aligned} \boldsymbol{\sigma}^i &= \boldsymbol{D}^i \boldsymbol{\varepsilon} + \hat{\boldsymbol{D}}^i \varepsilon_0 - \hat{\hat{\boldsymbol{D}}}^i \Delta T, \\ \sigma_{33}^i &= (\hat{\boldsymbol{D}}^i)^T \boldsymbol{\varepsilon} + (1 - \nu^i) C^i \varepsilon_0 - \frac{E^i \alpha^i}{1 - 2\nu^i} \Delta T, \end{aligned}\right\} \qquad i = f, m, \tag{18}$$

where f and m denote the fiber and the matrix, $\boldsymbol{\sigma} = \{\sigma_{11} \;\; \sigma_{22} \;\; \sigma_{12}\}^T$ is the stress tensor, σ_{33} is the axial stress in the fiber direction, $\boldsymbol{\varepsilon} = \{\varepsilon_{11} \;\; \varepsilon_{22} \;\; 2\varepsilon_{12}\}^T$ is the strain tensor, ε_0 is the constant strain in the fiber direction, $\boldsymbol{D}^i$, $\hat{\boldsymbol{D}}^i$, $\hat{\hat{\boldsymbol{D}}}^i$ are defined by

$$\boldsymbol{D}^i = C^i \begin{bmatrix} 1-\nu^i & \nu^i & 0 \\ \nu^i & 1-\nu^i & 0 \\ 0 & 0 & (1-2\nu^i)/2 \end{bmatrix}, \quad \hat{\boldsymbol{D}}^i = \nu^i C^i \begin{Bmatrix} 1 \\ 1 \\ 0 \end{Bmatrix}, \quad \hat{\hat{\boldsymbol{D}}}^i = \frac{E^i \alpha^i}{1-2\nu^i} \begin{Bmatrix} 1 \\ 1 \\ 0 \end{Bmatrix}. \tag{19}$$

Here E is the elastic modulus, ν is the Poisson's ratio, α is the coefficient of thermal expansion of the constituents, and

$$C^i = \frac{E^i}{(1-2\nu^i)(1+\nu^i)}.$$

Furthermore, the traction, $t_i = \sigma_{ij} n_j$ on the boundary of the support domain, $\partial\Omega_s^I$, in the matrix form can be obtained using (19) as

$$\boldsymbol{t} = \boldsymbol{N}\boldsymbol{\sigma} = \boldsymbol{N}\boldsymbol{D}\boldsymbol{\varepsilon} + \boldsymbol{N}\hat{\boldsymbol{D}}\varepsilon_0 - \boldsymbol{N}\hat{\hat{\boldsymbol{D}}}\Delta T. \tag{20}$$

By substituting (20) into (18) and using the MLS approximation (9), we obtain the discretized local weak form of governing equations (17):

$$-\sum_{J=1}^{N} \int_{L_s^I} \boldsymbol{N}\boldsymbol{D}\boldsymbol{B}^J \hat{\boldsymbol{u}}^J \, d\Gamma - \sum_{J=1}^{N} \int_{\Gamma_{su}^I} \boldsymbol{S}\boldsymbol{N}\boldsymbol{D}\boldsymbol{B}^J \hat{\boldsymbol{u}}^J \, d\Gamma + \beta \sum_{J=1}^{N} \int_{\Gamma_{su}^I} \boldsymbol{S}\boldsymbol{\Phi}^J \hat{\boldsymbol{u}}^J \, d\Gamma = \int_{\Omega_s^I} \boldsymbol{b} \, d\Omega + \int_{\Gamma_{st}^I} \bar{\boldsymbol{t}} \, d\Gamma$$
$$+ \varepsilon_0 \left(\int_{L_s^I} \boldsymbol{N}\hat{\boldsymbol{D}} \, d\Gamma + \int_{\Gamma_{su}^I} \boldsymbol{N}\hat{\boldsymbol{D}} \, d\Gamma \right) - \Delta T \left(\int_{L_s^I} \boldsymbol{N}\hat{\hat{\boldsymbol{D}}} \, d\Gamma + \int_{\Gamma_{su}^I} \boldsymbol{N}\hat{\hat{\boldsymbol{D}}} \, d\Gamma \right) + \beta \int_{\Gamma_{su}^I} \bar{\boldsymbol{u}} \, d\Gamma, \tag{21}$$

in which

$$\boldsymbol{B}^J = \begin{bmatrix} \phi_{,1}^J & 0 & \phi_{,2}^J \\ 0 & \phi_{,2}^J & \phi_{,1}^J \end{bmatrix}^T, \quad \boldsymbol{\Phi}^J = \begin{bmatrix} \phi^J & 0 \\ 0 & \phi^J \end{bmatrix}, \quad \boldsymbol{N} = \begin{bmatrix} n_1 & 0 & n_2 \\ 0 & n_2 & n_1 \end{bmatrix}, \quad \boldsymbol{S} = \begin{bmatrix} S_1 & 0 \\ 0 & S_2 \end{bmatrix}, \tag{22}$$

with (n_1, n_2) the outward unit normal vector to the boundary of the local subdomain $\partial\Omega_s^I$ and $\boldsymbol{S}$ the essential boundary conditions index (if u_i is prescribed on Γ_u, the index S_i is equal to 1; otherwise $S_i = 0$). Also, $\phi_{,i}^J$ is the partial derivative of $\phi^J(\boldsymbol{x})$ with respect to the x_i; details can be found in [Atluri and Shen 2002].

Equation (21) can be written in the standard form of linear algebraic equations in terms of $\hat{\boldsymbol{u}}^J$ as

$$\sum_{J=1}^{N} \boldsymbol{K}_{IJ} \hat{\boldsymbol{u}}^J = \boldsymbol{f}_I, \tag{23}$$

where

$$\boldsymbol{K}_{IJ} = -\int_{L_s^I} \boldsymbol{N}\boldsymbol{D}\boldsymbol{B}^J \, d\Gamma - \int_{\Gamma_{su}^I} \boldsymbol{S}\boldsymbol{N}\boldsymbol{D}\boldsymbol{B}^J \, d\Gamma + \beta \int_{\Gamma_{su}^I} \boldsymbol{S}\boldsymbol{\Phi}^J \, d\Gamma, \tag{24}$$

$$\boldsymbol{f}_I = \int_{\Gamma_{st}^I} \bar{\boldsymbol{t}} \, d\Gamma + \varepsilon_0 \left(\int_{\Gamma_s^I} \boldsymbol{N}\hat{\boldsymbol{D}} \, d\Gamma + \int_{\Gamma_{su}^I} \boldsymbol{N}\hat{\boldsymbol{D}} \, d\Gamma \right)$$
$$- \Delta T \left(\int_{\Gamma_s^I} \boldsymbol{N}\hat{\hat{\boldsymbol{D}}} \, d\Gamma + \int_{\Gamma_{su}^I} \boldsymbol{N}\hat{\hat{\boldsymbol{D}}} \, d\Gamma \right) + \beta \int_{\Gamma_{su}^I} \bar{\boldsymbol{u}} \, d\Gamma + \int_{\Omega_s^I} \boldsymbol{b} \, d\Omega. \tag{25}$$

It is worth mentioning that the stiffness matrix $\boldsymbol{K}_{IJ}$ in the present method is banded and asymmetric.

3.4. ***Material discontinuity.*** In order to treat the material discontinuity at the fiber and matrix interface, two sets of nodes are assigned on the interface at the same location with different material properties. One set is dedicated to the fiber denoted as I^f while the other set is related to the matrix denoted by I^m. Furthermore, a non-penetration rule is imposed to the influence domain of the nodes. This rule states that any point related to the matrix area cannot be influenced by the nodes in the fiber region and the fiber interface nodes, I^f and vise versa. This rule confines the influence domain of a node within the domain of the material of the same node. Finally, the displacement continuity and traction reciprocity conditions in (5) must be satisfied for the nodes on the interface as

$$\boldsymbol{u}^{I^f} = \boldsymbol{u}^{I^m}, \quad \boldsymbol{t}^{I^f} + \boldsymbol{t}^{I^m} = 0. \tag{26}$$

The discretized form of these equations for all interface nodes can be rewritten as

$$\sum_{J=1}^{N_f} (\boldsymbol{\Phi}^J(\boldsymbol{x}_{I^f})\hat{\boldsymbol{u}}^J)^f = \sum_{J=1}^{N_m} (\boldsymbol{\Phi}^J(\boldsymbol{x}_{I^m})\hat{\boldsymbol{u}}^J)^m, \tag{27}$$

$$\sum_{J=1}^{N_f} (\boldsymbol{N}\boldsymbol{D}\boldsymbol{B}^J\hat{\boldsymbol{u}}^J + \boldsymbol{N}\hat{\boldsymbol{D}}\boldsymbol{\varepsilon}_0 - \boldsymbol{N}\hat{\hat{\boldsymbol{D}}}\Delta T)^f = \sum_{J=1}^{N_m} (\boldsymbol{N}\boldsymbol{D}\boldsymbol{B}^J\hat{\boldsymbol{u}}^J + \boldsymbol{N}\hat{\boldsymbol{D}}\boldsymbol{\varepsilon}_0 - \boldsymbol{N}\hat{\hat{\boldsymbol{D}}}\Delta T)^m, \tag{28}$$

where N_f is the total nodes in the fiber and Nm is the total nodes in the matrix. In order to impose conditions (27) and (28) to the global stiffness and force matrix (23), the rows of the global stiffness and force matrix that are related to the interface nodes are replaced by the discretized form of the displacement and traction continuity equations (27) and (28). This leads to a direct implementation of the fiber-matrix interface conditions to the global system of equations.

4. Numerical results and discussion

The fabrication process of the composite materials, in particular metal-matrix composites (MMCs), takes place at high temperatures. Subsequently, when they are cooled down to room temperature, residual stresses are generated in the composite due to the mismatch between the coefficients of thermal expansion of the fiber and matrix. The generated residual stresses influence the overall thermomechanical properties of the composite. In the numerical results, the silicon carbide – titanium (SiC/Ti) metal-matrix composite

Composite system	Constituent	E (GPa)	ν	α $(10^{-6}/°C)$
SiC/Ti	SiC (fiber) Ti (matrix)	409 107	0.2 0.35	4.5 10
glass/epoxy	glass (fiber) epoxy (matrix)	72 3.5	0.2 0.35	5 52.5
[Shaw and Miracle 1996] [Nimmer et al. 1991]	Ti (fiber) SiC (matrix)	113.8 414	0.3 0.3	9.8 4.86

Table 1. Material properties of the fiber and matrix (E = Young's modulus; ν = Poisson's ratio; α = coefficient of thermal expansion).

and glass/epoxy polymer-matrix composite are studied. The composite constituents are assumed to be isotropic and homogeneous with the linear thermoelastic properties as shown in Table 1. To examine the efficiency and accuracy of the method, another analysis is carried out in the commercial finite element code ANSYS [2002].

In this session, the previously discussed micromechanical model with MLPG formulation is used to predict the process induced thermal residual stress in the SiC/Ti metal-matrix composite with 35% fiber volume fraction. The SiC/Ti composite is manufactured at the temperature of about 910°C that is assumed to be stress free temperature of this composite. At room temperature (25°C) the composite is subjected to a temperature change of about $\Delta T = -885$°C.

4.1. ***Pure thermal loading.*** The first step is to examine the rate of convergence of the method through a mesh sensitivity analysis. To this end, a 35% fiber volume fraction SiC/Ti composite system is subjected to a uniform thermal load of $\Delta T = -885$°C. Figure 2 shows the rate of convergence of the MLPG and ANSYS for the transverse displacement in the right side ($x_1 = a$) of the RVE in the x_1 direction. The results suggest that about 300 nodes are sufficient to provide final convergence in MLPG, while some 800 nodes are needed for convergence in FE analysis. Therefore, in order to maintain convergence, 350 and 1000 nodes, respectively, are used for all MLPG and FE results.

Thermal loading. The coefficient of thermal expansion (CTE) of the composite can be obtained by applying a pure thermal loading on the RVE. The CTE $\alpha_i = \varepsilon_i / \Delta T$ in the direction x_i is the quotient of the macroscopic total thermal strain ε_i in that direction by the applied thermal load ΔT. Figure 3 shows the longitudinal (α_3) and transverse ($\alpha_1 = \alpha_2$) CTE versus fiber volume fraction for a unidirectional glass/epoxy composite. Included in the figures are also predictions obtained by other approximate closed-form solutions [Van Fo Fy 1965; Rogers et al. 1977; Chamis 1984], FEM [Haktan Karadeniz and Kumlutas 2007] method and experimental measurements [Sideridis 1994]. It can be seen in the figures that predictions of the MLPG method are in the close agreement with the FEM and experiment for both longitudinal and transverse CTE. However, there are some discrepancies between the results of various approximate closed-form solutions in the transverse CTE of the glass/epoxy composite, mainly due to their various simplifying assumptions.

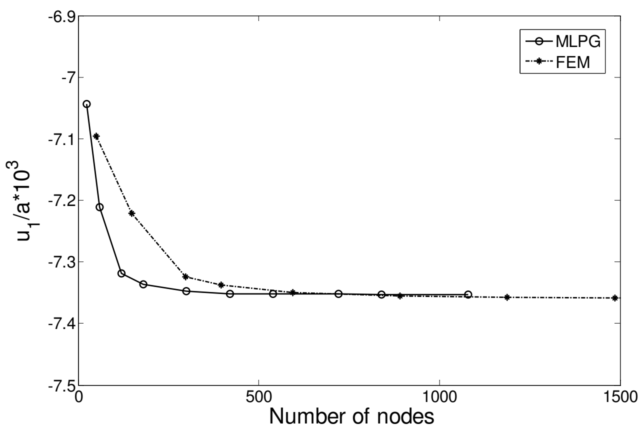

Figure 2. Convergence of u_1 displacement on the right side ($x_1 = a$) of the RVE.

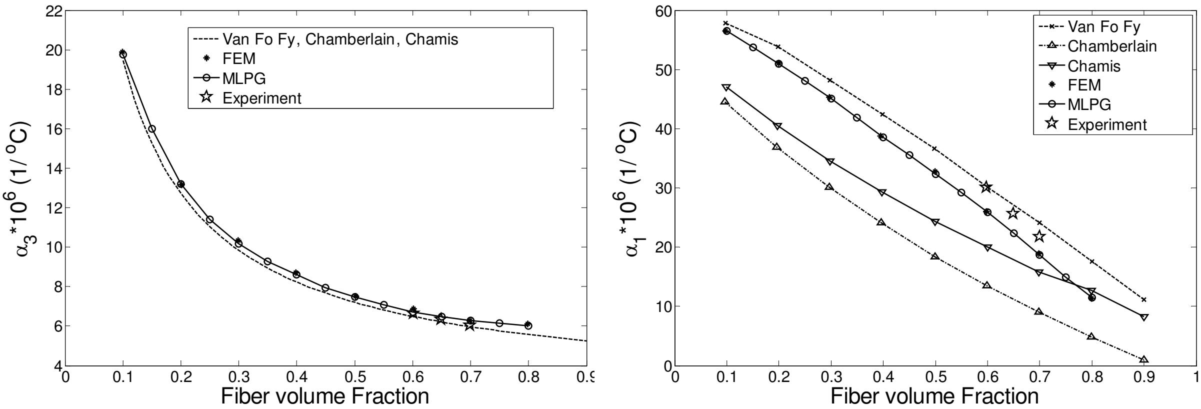

Figure 3. Longitudinal (left) and transverse (right) coefficients of thermal expansion of glass/epoxy composite. "FEM" and "Chamberlain" stand for the values in [Haktan Karadeniz and Kumlutas 2007] and "Experiment" for those in [Sideridis 1994].

Table 2 shows the CTE of SiC/Ti composite system predicted by MLPG, FE and approximate closed-form solutions [Van Fo Fy 1965; Rogers et al. 1977; Chamis 1984]. Again, very good agreement is seen between the results of MLPG and FE model while some differences exist in the predictions of approximate methods (loc. cit.), particularly in the transverse CTE.

We next consider the predicted manufacturing thermal residual stresses within the RVE of the SiC/Ti composite with 35% FVF induced by cooldown from 900°C to 25°C. Table 3 shows the stress components on the matrix side of the fiber-matrix interface at the point on the bottom edge of the RVE with coordinates $(R, 0)$. It also shows the results of ADINA finite element code presented in [Nimmer et al. 1991]. Discrepancies in the range from 5% to 10% are observed between the results there and ours. One possible reason for the discrepancies is that, in their FE analysis, Nimmer et al. regarded certain matrix properties as temperature-dependent, while we took them as temperature-independent in this study.

CTE	model	Fiber volume fraction 20%	35%	50%	60%	70%
$\alpha_1 = \alpha_2$	[Van Fo Fy 1965]	9.5400	8.7912	7.8989	7.2576	6.5916
	[Rogers et al. 1977]	8.3242	7.2080	6.1938	5.5678	4.9777
	[Chamis 1984]	9.7013	8.5327	7.2717	6.5074	5.8390
	[ANSYS 2002]	9.1705	8.3116	7.4112	6.7912	6.1264
	MLPG	9.1663	8.3058	7.4021	6.7815	6.0987
α_3	[Van Fo Fy 1965]	7.3124	6.2984	5.6405	5.3168	5.0545
	[ANSYS 2002]	7.4092	6.3981	5.7212	5.3812	5.1385
	MLPG	7.4006	6.3929	5.7164	5.3805	5.1322

Table 2. Coefficients of thermal expansion ($\times 10^6/°C$) of SiC/Ti metal-matrix composite, as predicted by approximate closed-form solutions (first three rows), FEM [ANSYS 2002] and the MLPG proposed here.

model	Radial stress σ_1 (MPa)	Hoop stress σ_2 (MPa)	Axial stress σ_3 (MPa)	Effective stress σ_{eff} (MPa)
MLPG	−329.8	559.7	395.3	819.8
FEM [Nimmer et al. 1991]	−314.2	509.8	371.90	760.5
discrepancy	4.96%	9.78%	6.29%	7.80%

Table 3. Thermal residual stress components on the matrix side of the interface at the point $(R, 0)$.

model	$\sigma_{1\,\max}$ at interface on x_1-axis	$\sigma_{2\,\max}$ in matrix near interface on diagonal line	σ_3 in fiber near interface on x_1-axis	$\sigma_{3\,\max}$ in matrix near interface on diagonal line	$\sigma_{3\,\min}$ in matrix near interface on x_1-axis
MLPG	−305.1	488.5	−779.8	354.2	310.4
FEM [Shaw and Miracle 1996]	−288	466	−782	354	316
discrepancy	5.93%	4.82%	−0.28%	0.056%	−1.77%

Table 4. Thermal residual stress (MPa) in SiC/Ti with 30% FVF system cool down from 800°C to 25°C.

Shaw and Miracle [1996] used ANSYS finite element code to study the SiC/Ti composite with 30% FVF cooled down from 800°C to 25°C. They used temperature-independent properties for fiber and matrix and considered a thin interfacial coating layer between the fiber and matrix. Table 4 compares their predictions for various thermal residual stresses with ours, showing reasonably good agreement.

Since the coefficient of thermal expansion of titanium is significantly higher than that of silicon carbide, it experiences greater contraction during cooldown, and relatively large radial compressive stresses build up at the fiber-matrix interface. The dimensionless displacements u_1/a at the bottom $(x_2 = 0)$ and top path $(x_2 = a)$ of the RVE induced during the cooling from 910°C to 25°C are shown in Figure 4. This

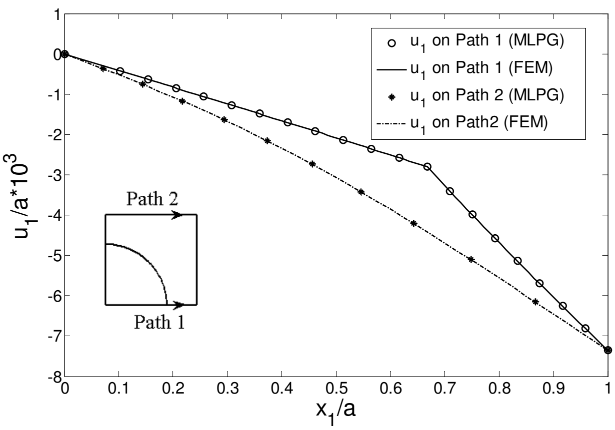

Figure 4. Displacement u_1 on the bottom path $(x_2 = 0)$ and top path $(x_2 = a)$ of the RVE in SiC/Ti composite after cooling; $\Delta T = -885$°C.

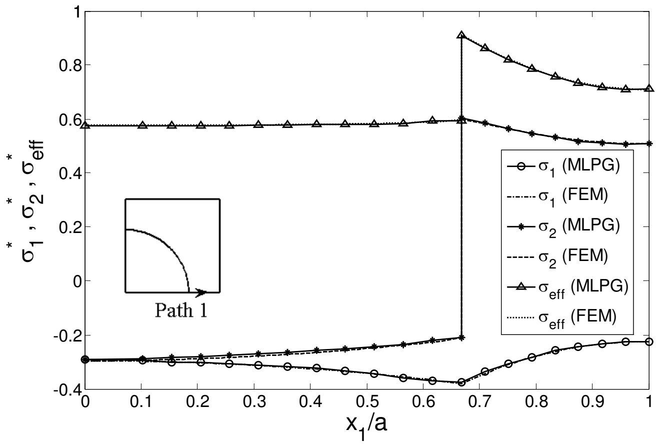

Figure 5. Distribution of thermal residual stresses σ_1^*, σ_2^* and σ_{eff}^* on the bottom path 1 of the RVE, $\Delta T = -885°\text{C}$.

figure includes the prediction of MLPG and ANSYS code. It is seen that the RVE contracts about 0.735% in transverse direction after cooling. On the bottom path, the slope of displacement in the matrix (Ti) is higher than that of fiber (SiC). It is clear that the MLPG method presented here is in appropriate agreement with FEM in the prediction of displacement distribution within the RVE. Both MLPG and FEM predict continuous displacement in the fiber-matrix interface. The contraction of the RVE in the fiber direction predicted by MLPG and FEM is 0.7350% and 0.7355%, respectively.

The distribution of dimensionless normal residual stresses σ_1^* and σ_2^* and effective von Mises stress σ_{eff}^* on the bottom path (x_1-axis) of the RVE is shown in Figure 5. In this study the dimensionless stress is defined as $\sigma^* = \sigma / Y_m$, where Y_m is the yield stress of Ti and taken $Y_m = 910\,\text{MPa}$. It is obvious that along the bottom path, the σ_1 stress is the radial stress and σ_2 stress is the hoop stress.

As expected, because the CTE of Ti is higher than of SiC, on the bottom path the σ_1^* stress is compressive in both fiber and matrix and is continuous at the fiber-matrix interface. On the bottom path, the σ_2^* stress is compressive in fiber, is tensile in the matrix, and is discontinuous at fiber matrix interface. As seen in Figure 5, although the effective stress induced through the cooling is large, it does not exceed the yield stress of the matrix and no yielding occurs during the cooling. The figure suggests excellent agreement between the MLPG predictions and the ANSYS results.

The distributions of the residual circumferential stress σ_θ^*, normal stress σ_n^* and shear stress $\sigma_{n\theta}^*$ at the fiber-matrix interface are shown in Figure 6. At the interface, σ_θ^* is compressive in the fiber and is tensile in the matrix. The tensile σ_θ stress in the matrix may cause micro cracks in the matrix normal to the interface. The radial stress is compressive on entire interface and reaches its greatest value, about $-337\,\text{MPa}$, at $\theta = 0$ and $\theta = 90°$. The compressive residual stress at the fiber-matrix interface has a beneficial effect on the transverse behavior of the MMC with a weak interface [Nimmer 1990; Nimmer et al. 1991; Wisnom 1990].

In order to illustrate the accuracy of our MLPG method over the entire domain, the spatial variation of residual von Mises effective stress (σ_{eff}) predicted by the MLPG model and an FEM model are visualized in Figure 7. It can be seen that the pattern of the stress distribution is completely similar in MLPG and

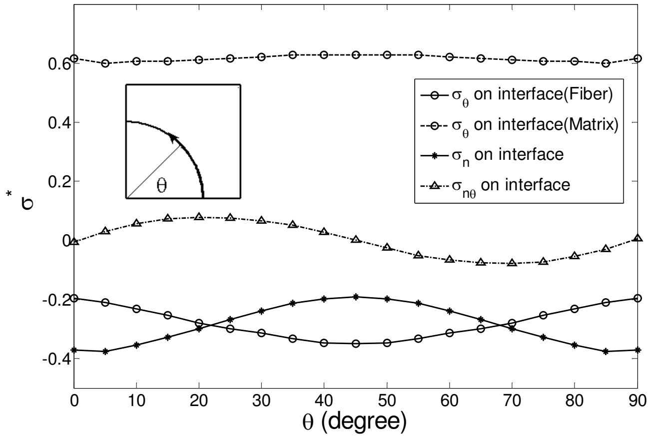

Figure 6. Distribution of dimensionless thermal residual stress σ_θ^*, σ_n^* and $\sigma_{n\theta}^*$ on the interface, $\Delta T = -885°C$.

FEM analysis. The effective stress in the fiber is uniform, about 527 MPa, and in the matrix varies from less than 300 MPa to more than 750 MPa. The largest value of the effective stress occurs at the fiber-matrix interface on the x_1-axis and x_2-axis. These locations are along the radial lines between closest neighbor fibers. The lowest effective stress is in top-right corner ($x_1 = x_2 = a$) of the RVE which is along the radial line between most distant neighbor fibers.

The radial residual stress σ_r^* is compressive in the fiber and the circumferential (hoop) stress σ_θ^* is compressive in the fiber and is tensile in the matrix. The axial stress σ_3^* in the fiber and matrix is fairly uniform and is compressive in the fiber and is tensile in the matrix. In the absence of axial load, the net force from the integration of local distribution of σ_3 over the entire face of the RVE is zero for any temperature distribution. The axial stress σ_3 on the fiber is almost uniform, with values between -793 and -782 MPa.

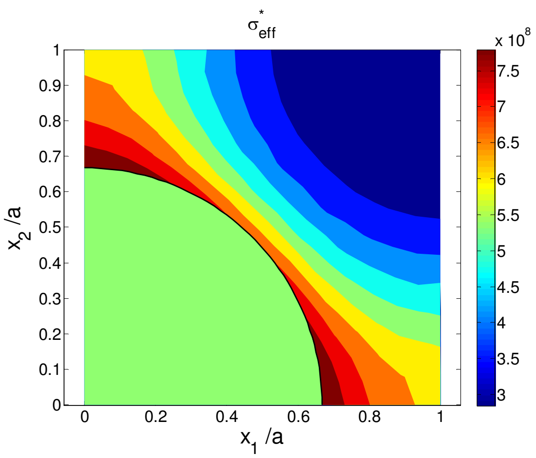

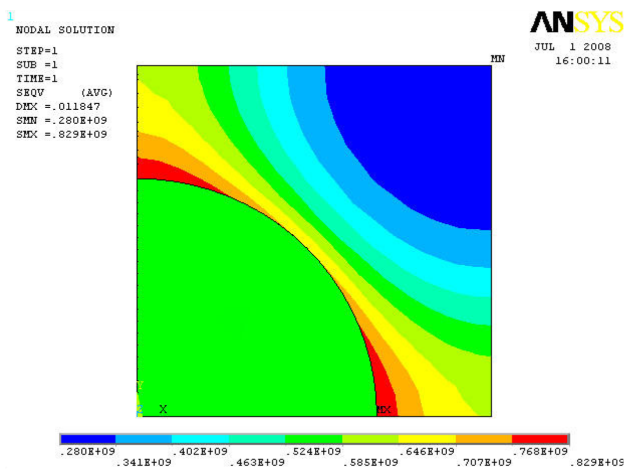

Figure 7. Distribution of von Mises effective stress σ_{eff} in the RVE, $\Delta T = -885°C$, as predicted by MLPG (left) and ANSYS (right).

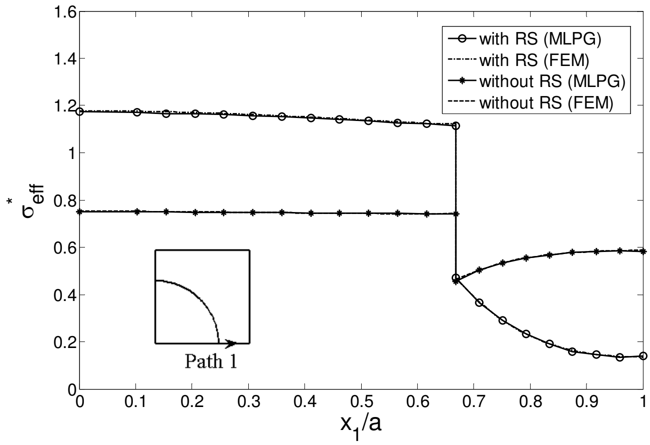

Figure 8. Dimensionless stress σ^*_{eff} on the bottom path for uniaxial tensile load $\bar{\sigma}_1 = +0.5Y_m$ with and without consideration of thermal residual stress.

4.2. *Thermomechanical loading.* In this section, the effect of thermal residual stress in the behavior of SiC/Ti system with 35% FVF under transverse mechanical normal loading is studied.

Transverse uniaxial loading. First, it is supposed that the SiC/Ti composite system is subjected to an external transverse tensile macro-stress $\bar{\sigma}_1 = 0.5Y_m = 455$ MPa in the x_1 direction. Figure 8 shows the distribution of σ^*_{eff} stress on the bottom path of the RVE with and without considering the thermal residual stress using the MLPG and the FE method. It is seen in the figure that in the presence of residual stress, the von Mises effective stress on the bottom path is increased in the fiber and is decreased in the matrix. Very close agreement is seen between the results of the present method and FEM analysis. It is concluded that our MLPG method has appropriate accuracy in the prediction of thermomechanical behavior of composite materials. The effect of the presence of thermal residual stress on the distribution of the dimensionless normal σ^*_n and shear stress $\sigma^*_{n\theta}$ at the fiber-matrix interface are shown in Figure 9.

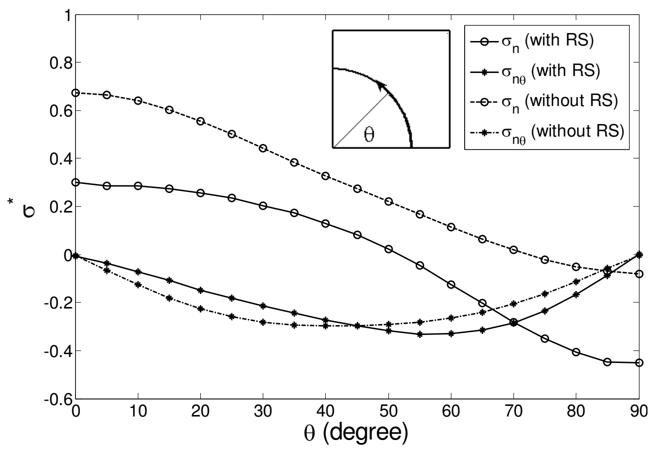

Figure 9. Dimensionless stress σ^*_n and $\sigma^*_{n\theta}$ on the interface for uniaxial tensile load $\bar{\sigma}_1 = +0.5Y_m$, considering thermal residual stress.

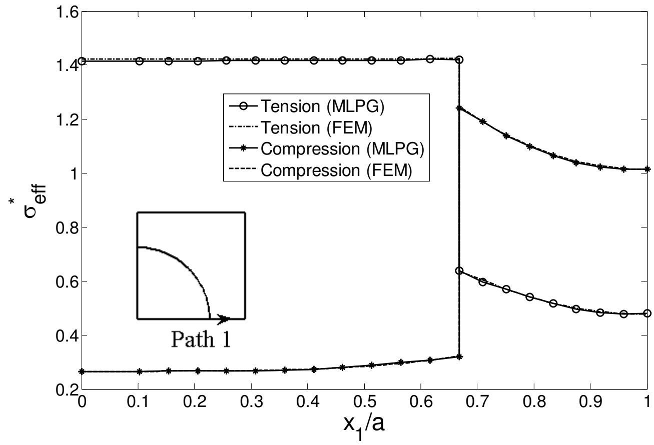

Figure 10. Dimensionless stress σ^*_{eff} on the bottom Path 1 of the RVE, biaxial tensile and compressive load $\bar{\sigma}_1 = \bar{\sigma}_2 = \pm 0.5Y_m$ with considering thermal residual stress.

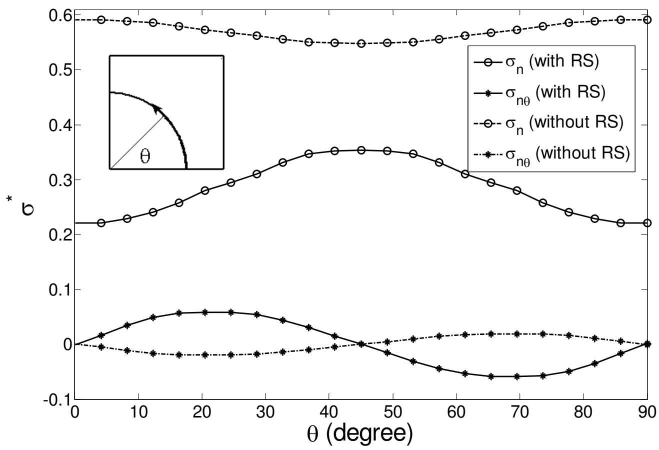

Figure 11. Dimensionless stress σ^*_n and $\sigma^*_{n\theta}$ on the interface for biaxial tensile load $\bar{\sigma}_1 = \bar{\sigma}_2 = +0.5Y_m$, -Effect of thermal residual stress.

The maximum value of the normal to interface stress σ_n is decreased in the presence of thermal residual stress from 611.4 to 274.1 MPa. Therefore, thermal residual stresses have beneficial effect for metal-matrix composite with weak interface bonding [Nimmer 1990; Nimmer et al. 1991; Wisnom 1990].

Transverse biaxial loading. The behavior of the SiC/Ti composite with 35% FVF under biaxial transverse loading in presence of thermal residual stress is studied. For this case, the equal transverse normal tensile $\bar{\sigma}_1 = \bar{\sigma}_2 = +0.5Y_m$ and compressive $\bar{\sigma}_1 = \bar{\sigma}_2 = -0.5Y_m$ stresses are applied to the SiC/Ti composite system. Figure 10 shows the distribution of the dimensionless effective stress σ^*_{eff} on the bottom path of the RVE in the biaxial transverse tension and compression in the presence of thermal residual stress. It is seen that the von Mises effective stress in tension and compression does not have the same values. This will cause asymmetric yielding behavior for SiC/Ti MMC in the transverse tension and compression. In addition, it is seen that in the matrix the effective stress σ^*_{eff} for compressive transverse load is bigger than for the same tensile load. Therefore, it can be concluded that the smaller compressive transverse load will cause yielding of SiC/Ti composite in comparison with the transverse tensile load.

The distributions of the dimensionless normal to fiber-matrix interface stress σ_n^* and shear stress on interface $\sigma_{n\theta}^*$ are shown in Figure 11. The stresses on the interface have symmetry respect to $\theta = 45°$. Thermal residual stresses change the location of maximum of σ_n from $\theta = 0$ and $\theta = 90°$ to $\theta = 45°$. In the presence of thermal residual stress the σ_n stress on x_1- and x_2-axis ($\theta = 0$ and $\theta = 90°$) decreases from 538.3 to 200.7 MPa and at the location $\theta = 45$ is decreased from 499.1 to 321.9 MPa.

5. Conclusion

An appropriate meshless local Petrov–Galerkin method is presented for micromechanical modeling of the unidirectional composites subjected to various thermomechanical loadings. Generalized plane strain assumption in the context of theory of elasticity is used to obtain the governing partial differential equations of the problem. A direct method is introduced for the treatment of material discontinuity at the fiber-matrix interface in which both the displacement continuity and traction reciprocity are satisfied. This MLPG method together with the MLS approximation is employed to obtain a solution for the governing equations over the selected RVE with appropriate boundary conditions. The computational time is substantially reduced by employing the unit step function as the test function. The accuracy and convergence rate of the method for micromechanical analysis of unidirectional composite is investigated. The mesh sensitivity analysis revealed that in comparison with the finite element analysis, the method presented provides highly accurate results with relatively small number of nodes. Comparison of the coefficient of thermal expansion, displacement and stress components distribution with experimental, numerical and analytical methods shows good agreement.

References

[Adams and Doner 1967] D. F. Adams and D. R. Doner, "Transverse normal loading of a unidirectional composite", *J. Compos. Mater.* **1**:2 (1967), 152–164.

[Aghdam and Khojeh 2003] M. M. Aghdam and A. Khojeh, "More on the effects of thermal residual and hydrostatic stresses on yielding behavior of unidirectional composites", *Compos. Struct.* **62**:3–4 (2003), 285–290.

[Aghdam et al. 2000] M. M. Aghdam, D. J. Smith, and M. J. Pavier, "Finite element micromechanical modelling of yield and collapse behaviour of metal matrix composites", *J. Mech. Phys. Solids* **48**:3 (2000), 499–528.

[ANSYS 2002] *ANSYS documentation*, ANSYS, Inc., Canonsburg, PA, 2002, Available at http://www.ansys.com/services/ss-documentation-manuals.asp.

[Arsenault and Taya 1987] R. J. Arsenault and M. Taya, "Thermal residual stresses in metal matrix composite", *Acta Metall.* **35**:3 (1987), 651–659.

[Atluri and Shen 2002] S. N. Atluri and S. Shen, *The meshless local Petrov–Galerkin (MLPG) method*, Tech Science Press, Encino, CA, 2002.

[Atluri and Zhu 1998] S. N. Atluri and T. Zhu, "A new meshless local Petrov–Galerkin (MLPG) approach in computational mechanics", *Comput. Mech.* **22**:2 (1998), 117–127.

[Atluri and Zhu 2000] S. N. Atluri and T. Zhu, "The meshless local Petrov–Galerkin (MLPG) approach for solving problems in elasto-statics", *Comput. Mech.* **25**:2–3 (2000), 169–179.

[Belytschko et al. 1994] T. Belytschko, Y. Y. Lu, and L. Gu, "Element-free Galerkin methods", *Int. J. Numer. Methods Eng.* **37**:2 (1994), 229–256.

[Brayshaw and Pindera 1994] J. B. Brayshaw and M.-J. Pindera, "The effect of matrix constitutive model on residual thermal stresses in MMC", *J. Eng. Mater. Technol. (ASME)* **116**:4 (1994), 505–511.

[Chamis 1984] C. C. Chamis, "Simplified composite micromechanics equations for hygral, thermal and mechanical properties", *SAMPE Q.* **15**:3 (1984), 14–23.

[Ching and Batra 2001] H.-K. Ching and R. C. Batra, "Determination of crack tip fields in linear elastostatics by the meshless local Petrov–Galerkin (MLPG) method", *Comput. Model. Eng. Sci.* **2**:2 (2001), 273–290.

[Dang and Sankar 2007] T. D. Dang and B. V. Sankar, "Meshless local Petrov–Galerkin for problems in composite micromechanics", *AIAA J.* **45**:4 (2007), 912–921.

[Durodola and Derby 1994] J. F. Durodola and B. Derby, "An analysis of thermal residual stresses in Ti-6-4 alloy reinforced with SiC and Al_2O_3 fibres", *Acta Metall. Mater.* **42**:5 (1994), 1525–1234.

[Dvorak et al. 1973] G. J. Dvorak, M. S. M. Rao, and J. Q. Tarn, "Yielding in unidirectional composites under external loads and temperature changes", *J. Compos. Mater.* **7**:2 (1973), 194–216.

[Eischen and Torquato 1993] J. W. Eischen and S. Torquato, "Determining elastic behavior of composites by the boundary element method", *J. Appl. Phys.* **74**:1 (1993), 159–170.

[Gentz et al. 2004] M. Gentz, B. Benedikt, J. K. Sutter, and M. Kumosa, "Residual stresses in unidirectional graphite fiber/polyimide composites as a function of aging", *Compos. Sci. Technol.* **64**:10–11 (2004), 1671–1677.

[Gramoll et al. 1991] K. C. Gramoll, K. P. Walker, and A. D. Freed, "An overview of self-consistent methods for fiber reinforced composites", NASA Technical Memorandum 103713, Lewis Research Center, Cleveland, OH, 1991, Available at http://tinyurl.com/NASA-TM-103713.

[Gu and Liu 2001] Y. T. Gu and G. R. Liu, "A meshless local Petrov–Galerkin (MLPG) formulation for static and free vibration analyses of thin plates", *Comput. Model. Eng. Sci.* **2**:4 (2001), 463–476.

[Haktan Karadeniz and Kumlutas 2007] Z. Haktan Karadeniz and D. Kumlutas, "A numerical study on the coefficients of thermal expansion of fiber reinforced composite materials", *Compos. Struct.* **78**:1 (2007), 1–10.

[Lin and Atluri 2001] H. Lin and S. N. Atluri, "The meshless local Petrov–Galerkin (MLPG) method for solving incompressible Navier–Stokes equations", *Comput. Model. Eng. Sci.* **2**:2 (2001), 117–142.

[Liu et al. 1996] W. K. Liu, Y. Chen, C. T. Chang, and T. Belytschko, "Advances in multiple scale kernel particle methods", *Comput. Mech.* **18**:2 (1996), 73–111.

[Long et al. 2006] S. Y. Long, K. Y. Liu, and D. A. Hu, "A new meshless method based on MLPG for elastic dynamic problems", *Eng. Anal. Bound. Elem.* **30**:1 (2006), 43–48.

[Nayroles et al. 1992] B. Nayroles, G. Touzot, and P. Villon, "Generalizing the finite element method: diffuse approximation and diffuse elements", *Comput. Mech.* **10**:5 (1992), 307–318.

[Nimmer 1990] R. P. Nimmer, "Fiber-matrix interface effects in the presence of thermally induced residual stress", *J. Compos. Tech. Res.* **12**:2 (1990), 65–75.

[Nimmer et al. 1991] R. P. Nimmer, R. J. Bankert, E. S. Russell, G. A. Smith, and P. K. Wright, "Micromechanical modeling of fiber/matrix interface effects in transversely loaded SiC/Ti-6-4 metal matrix composites", *J. Compos. Tech. Res.* **13**:1 (1991), 3–13.

[Rogers et al. 1977] K. F. Rogers, L. N. Phillips, D. M. Kingston-Lee, B. Yates, M. J. Overy, J. P. Sargent, and B. A. McCalla, "The thermal expansion of carbon fibre-reinforced plastics, 1: The influence of fibre type and orientation", *J. Mater. Sci.* **12**:4 (1977), 718–734.

[Shaw and Miracle 1996] L. L. Shaw and D. B. Miracle, "Effects of an interfacial region on the transverse behavior of metal-matrix composites: a finite element analysis", *Acta Mater.* **44**:5 (1996), 2043–2055.

[Shen 1998] Y.-L. Shen, "Thermal expansion of metal-ceramic composites: a three-dimensional analysis", *Mater. Sci. Eng. A* **252**:2 (1998), 269–275.

[Sideridis 1994] E. Sideridis, "Thermal expansion coefficients of fiber composites defined by the concept of the interphase", *Compos. Sci. Technol.* **51**:3 (1994), 301–317.

[Tsai and Chi 2008] J.-L. Tsai and Y.-K. Chi, "Investigating thermal residual stress effect on mechanical behaviors of fiber composites with different fiber arrays", *Compos. B Eng.* **39**:4 (2008), 714–721.

[Uemura et al. 1979] M. Uemura, H. Iyama, and Y. Yamaguchi, "Thermal residual stresses in filament-wound carbon-fiber-reinforced composites", *J. Therm. Stresses* **2**:3–4 (1979), 393–412.

[Van Fo Fy 1965] G. A. Van Fo Fy, "Elastic constants and thermal expansion of certain bodies with inhomogeneous regular structure", *Dokl. Akad. Nauk SSSR* **166** (1965), 817. In Russian; translated in *Sov. Phys. Dokl.* **11** (1966), 176.

[Wisnom 1990] M. R. Wisnom, "Factors affecting the transverse tensile strength of unidirectional continuous silicon carbide fibre reinforced 6061 aluminum", *J. Compos. Mater.* **24**:7 (1990), 707–726.

[Yeh and Krempl 1993] N.-M. Yeh and E. Krempl, "The influence of cool-down temperature histories on the residual stresses in fibrous metal-matrix composites", *J. Compos. Mater.* **27**:10 (1993), 973–995.

[Zahl and McMeeking 1991] D. B. Zahl and M. R. McMeeking, "The influence of residual stress on the yielding of metal matrix composites", *Acta Metall. Mater.* **39**:6 (1991), 1117–1122.

[Zhang et al. 2004] Y. Zhang, Z. Xia, and F. Ellyin, "Evolution and influence of residual stresses/strains of fiber reinforced laminates", *Compos. Sci. Technol.* **64**:10–11 (2004), 1613–1621.

[Zhao et al. 2007] L. G. Zhao, N. A. Warrior, and A. C. Long, "A thermo-viscoelastic analysis of process-induced residual stress in fibre-reinforced polymer-matrix composites", *Mater. Sci. Eng. A* **452–453** (2007), 483–498.

[Zhu et al. 1998] T. Zhu, J.-D. Zhang, and S. N. Atluri, "A local boundary integral equation (LBIE) method in computational mechanics, and a meshless discretization approach", *Comput. Mech.* **21**:3 (1998), 223–235.

Received 26 Apr 2009. Revised 30 Nov 2009. Accepted 7 Dec 2009.

ISA AHMADI: i_ahmadi@aut.ac.ir
Department of Mechanical Engineering, Amirkabir University of Technology, Tehran 15914, Iran

MOHAMAD AGHDAM: aghdam@aut.ac.ir
Thermoelasticity Center of Excellency, Department of Mechanical Engineering, Amirkabir University of Technology, Tehran 15914, Iran

JOURNAL OF MECHANICS OF MATERIALS AND STRUCTURES

http://www.jomms.org

Founded by Charles R. Steele and Marie-Louise Steele

Cover design: Alex Scorpan

Cover photo: Mando Gomez, www.mandolux.com

See inside back cover or http://www.jomms.org for submission guidelines.

JoMMS (ISSN 1559-3959) is published in 10 issues a year. The subscription price for 2010 is US $500/year for the electronic version, and $660/year (+$60 shipping outside the US) for print and electronic. Subscriptions, requests for back issues, and changes of address should be sent to Mathematical Sciences Publishers, Department of Mathematics, University of California, Berkeley, CA 94720–3840.

JoMMS peer-review and production is managed by EditFlow™ from Mathematical Sciences Publishers.

PUBLISHED BY

mathematical sciences publishers

http://www.mathscipub.org

A NON-PROFIT CORPORATION

Typeset in LaTeX

Journal of Mechanics of Materials and Structures

Volume 5, No. 4 April 2010